Characterizations of Spherical Luneburg Lens Antennas with Air-gaps and Dielectric Losses

Kang Wook Kim

Abstract

In this paper, spherical Luneburg lens antennas have been systematically analyzed using the Eigenfunction Expansion Method (EEM). The developed technique has capability of performing a complete 3-D analysis to characterize the multi-layered dielectric spherical lens with arbitrary permittivity and permeability. This paper describes the analysis technique, and presents the results of the parametric study of Luneburg lens antennas by varying design parameters such as the diameter of the lens antenna (up to 80 wavelength), number of spherical shells (up to 30 shells), air-gaps between spherical shells, and dielectric loss of the material. Many representative engineering design curves including the far-field patterns, wide-angle sidelobe characterizations, antenna efficiency have been presented.

Key words : Luneburg lens, lens antenna, dyadic green's function, EM scattering

I. INTRODUCTION

Recently, Luneburg lens antennas regain interests in their applications of multi-beam scanning for use in the mm-wave automotive radars, present-day military, and satellite-based mobile -communications[1]~[4]. In principle, a Luneburg lens transforms a point source radiation into a plane wave by correcting the phase of the source[5]~[7]. Since the foundation principle of the Luneburg lens is based on the geometrical optics concept, the lens antenna can be operated with broad frequency bandwidth, usually limited by the bandwidth of feed sources. Also, the spherical symmetry of the lens allows multiple beam scanning by means of an array of feeds placed around the lens surface. Due to these attractive features, the concept of the lens has been extensively studied in late 1950s and early 1960s[8]~[11]. With the advent of phased array antennas which allow fast and wide-angle beam scanning by electronically controlling antenna -element phases, the practical applications of the Luneburg lens has become very limited. However, due to modern communi-cation system links requiring broad frequency bands and multiple targets, the interests in the Luneburg lens have been rekindled[4]. While both the Luneburg lens antenna and the phased array antenna allow fast multi-beam scanning, phased array antennas typically operate at much narrower frequency bandwidth than Luneburg lens antennas. Due to its ray optical collimating feature, the Luneburg lens antenna also shares similar performance to the reflector antenna with the same aperture size.

An ideal Luneburg lens antenna consists of a dielectric sphere with continuously-varying relative permittivity from $\varepsilon_r = 1$ at the outer edge to $\varepsilon_r = 2$ at the center of the sphere; i.e., $\varepsilon_r = 2 -$

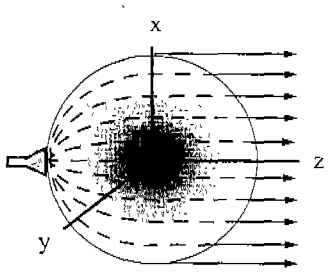

$\varepsilon_r = 2 - (r/a)^2$

(a)

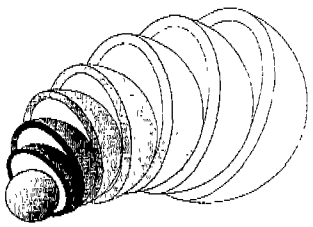

$\varepsilon_{r,n} = 2 - [(r_{n-1}+r_n)/2a]^2$

(b)

Fig. 1. (a) An ideal Luneburg lens antenna with continuous permittivity, (b) practical Luneburg lens antenna made of N concentric shells with permittivity of $\varepsilon_{r,n}$ for the n-the shell.

Manuscript received January 26, 2001; revised March 3, 2001.

Kang Wook Kim is with the Narda DBS Microwave - an L-3 Communications Company, 4805 Golden Foothill Parkway, El Dorado Hills, CA 95762, Work (016) 939-7545, E-mail : kang.kim@L-3com.com

$(r/a)^2$ where a is the radius of the sphere (see Fig. 1(a)).[6] In practice, however, the Luneburg lens antenna is constructed with a finite number of concentric spherical shells, which approximate the continuous variation of the permittivity as illustrated in Fig. 1(b). There are several variations in the implementation of the Luneburg lens, but, in this paper, the thickness of the spherical shell is kept constant, which may be the most practical choice in the view of its implementation. The dielectric properties for each shell, with the relative permittivity varying from 1 to 2, can be obtained by expanding polystyrene and polyethylene beads[1].

In this paper, design characterizations of Luneburg lens antennas have been presented using a complete 3-D analysis computer code based on the eigenfunction expansion method (EEM). To create realistic configurations, Luneburg lens antennas with air-gaps and dielectric losses have been analyzed for the gain, aperture efficiency, and far field. Many useful observations have been made as to the performance of Luneburg lens antennas. The formulation of the analysis has been systematically derived from the dyadic Green's functions of the multi-layered sphere[3],[6],[12]. The implemented computer code can handle a Luneburg lens with a diameter in excess of 80 wavelengths and more than 30 spherical shells, which may completely cover practical design interests of Luneburg lens antennas. It is worthwhile to mention that this computer code has been extensively validated with the published results, and also used in investigating electromagnetic interactions between antennas and a human head[13].

The rest of this paper is as follows: Section II briefly discusses the analysis technique based on the eigenfunction expansion method. Section III presents characterizations of the Luneburg lens antennas as a function of various parameters such as the number of shells, lens diameter, air-gaps, and dielectric loss. Section IV concludes this paper.

II. ANALYSIS TECHNIQUE AND NUMERICAL CONVERGENCE

The eigenfunction expansion method (EEM) is based on the exact scattering solution of infinitesimal dipoles in the presence of a multi-layered sphere. The total electric field at any observation location in the presence of a scattering object can be decomposed into the incident field and the scattered field. For the calculation of the incident field, the closed-form analytical expression is used for efficient computations; the scattered field is expressed as a series expansion of the spherical vector wave functions[12]. Fig. 2(a) illustrates the geometry of the multi-layered Luneburg lens consisting of N spherical regions with the corresponding constitutive parameters. The scattered field expressions can be obtained through the dyadic Green's function

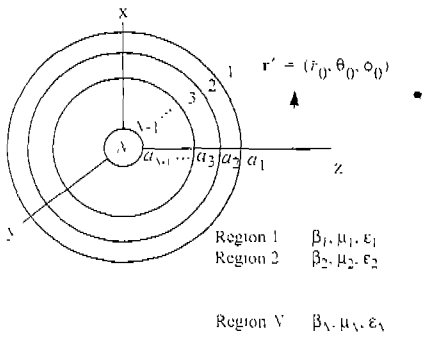

(a)

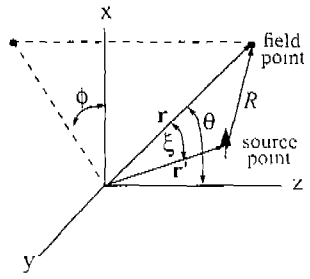

(b)

Fig. 2. Geometry of an N-layered Luneburg lens: (a) an N-layered dieledtric sphere. β is the propagation constant, μ the permeability, and ε the permittivity; (b) spherical coordinates, centered at the origin of the lens, for field computation.

approach for an infinitesimal electric dipole in the presence of a multi-layered sphere. In general, lens feeds can be modeled as superposition of many infinitesimal dipoles.

Using the dyadic Green's functions in terms of spherical vector wave functions[12], the total electric field can be obtained for Region p $(a_p \le r \le a_{p-1})$ where $p = 1, 2, \ldots, N$ as

$$\boldsymbol{E}_p(\boldsymbol{r}) = -\left(\frac{\omega\mu_1 Il}{4\pi}\cdot\beta_1\right)\sum_{n=1}^{\infty}\sum_{m=0}^{n}(2-\delta_{m0})\frac{(2n+1)(n-m)!}{n(n+1)(n+m)!}\cdot \left\{\begin{array}{l}\left(A_{n,p}\mathbf{M}^{(1)}_{\substack{e\\o}mn}(\beta_p)+C_{n,p}\mathbf{M}^{(1)}_{\substack{e\\o}mn}(\beta_p)\right)\left[\mathbf{M}^{(4)'}_{\substack{e\\o}mn}(\beta_1)\cdot\mathbf{p}\right]+\\ \left(B_{n,p}\mathbf{N}^{(4)}_{\substack{e\\o}mn}(\beta_p)+D_{n,p}\mathbf{N}^{(1)}_{\substack{e\\o}mn}(\beta_p)\right)\left[\mathbf{N}^{(1)}_{\substack{e\\o}mn}(\beta_1)\cdot\mathbf{p}\right]\end{array}\right\} \quad (1)$$

where

$$\delta_{m0} = \begin{cases} 1 & m=0 \\ 1 & m\neq 0 \end{cases} \text{ (Kronecker delta function)} \quad (2a)$$

$$\beta_p = \omega\sqrt{\mu_p\varepsilon_p} \text{ (Propagation constant)} \quad (2b)$$

$\mathbf{p}$ is the unit vector of the electric dipole; $\mathbf{M}^{(i)}_{\substack{e\\o}mn}(\beta_p)$ and $\mathbf{N}^{(i)}_{\substack{e\\o}mn}(\beta_p)$ are spherical vector wave functions (even or odd mode) defined in [12], and primed components are evaluated at the source location.

The expansion coefficients $A_{n,p}$, $B_{n,p}$, $C_{n,p}$, and $D_{n,p}$ in (1) can

be obtained by applying boundary conditions to the tangential electric and magnetic fields at the dielectric interfaces ($r = a_p$). The boundary conditions for the dielectric sphere impinged upon by an infinitesimal dipole radiation can be expressed in terms of dyadic Green's functions[12].

$$\mathbf{r} \times \overline{\mathbf{G}}_e^{(p,l)} \mid_{r=a_p} = \mathbf{r} \times \overline{\mathbf{G}}_e^{(p,l+1)} \mid_{r=a_{p+1}} \tag{3a}$$

$$\frac{1}{\mu_p} \mathbf{r} \times \nabla \times \overline{\mathbf{G}}_e^{(p,l)} \mid_{r=a_p} = \frac{1}{\mu_{p+1}} \mathbf{r} \times \nabla \times \overline{\mathbf{G}}_e^{(p,l+1)} \mid_{r=a_{p+1}} \tag{3b}$$

Equations (3a) and (3b) result in two simultaneous equations, from which the expansion coefficients can be successively solved in a cascaded analysis[14]. It should be noted that, in (1), $C_{n,1} = 1$ to match the incident radiation and $A_{n,N} = 0$ to avoid infinite field at the origin. Similarly, it is required that $D_{n,1} = 1$ and $B_{n,N} = 0$.

As can be seen in (1), the scattered fields are expressed as an infinite sum of spherical vector wave functions. In practice, however, series terms are truncated for the required accuracy. One way to define the required number of series terms at each field point is to determine whether the ratio between the q-th term and the total series sum up to (q-1) th term is less than a specified error. The series convergence properties depend on source locations, field-point locations, and the size of the spheres. For example, if an electric dipole, oriented in the x-direction, is located at 1 λ away from the surface of a homogeneous dielectric sphere, the required n series terms for far-field calculations with 10^{-6} accuracy level can be obtained as ~75 terms for a 20-λ sphere, ~150 terms for a 40-λ sphere, and ~220 terms for a 60-λ sphere. For near field calculation, more series terms are required for a given accuracy. In addition, if the dipole source is located closer to the sphere (e.g., 0.1 λ away from the sphere), much more series terms are required. Therefore, in the numerical implementation, the required series term for each observation point should be adaptively determined in order to satisfy the accuracy level.

Ⅲ. CHARACTERIZATIONS of LUNEBURG LENS ANTENNAS

In practice, a Luneburg lens antenna is simulated by multiple dielectric spherical shells as shown in Fig. 3(a). In this paper, an end-fire feed source with four infinitesimal dipoles is used to create the radiation characteristics of a typical feed with reasonable back radiation. The infinitesimal dipoles are oriented in the x-direction and located in the y-z plane. The feed gain patterns in the x-z and y-z planes are shown in Fig. 3(b), and the directivity of the feed array source is ~8.5 dB. With this feed, the backward spill-over power is ~7 % of the total radiated power.

In the following calculation, the gain, G, is defined as

$$G = 4\pi \frac{\text{Radiation Intensity}}{\text{Total Input Power}} \tag{4}$$

and the aperture efficiency, ε_{ap}, for a circular aperture is obtained as

$$\varepsilon_{ap} = \frac{\text{Maximum Effective Area}}{\text{Physical Area}} = \frac{G}{\pi^2 (L/\lambda)^2} \tag{5}$$

where L is the diameter of the circular aperture.

3-1 Effects of Number of Shells and Lens Diameter

For a Luneburg lens antenna with a fixed diameter, the gain and aperture efficiency of the lens antenna tend to improve by increasing the number of shells. This is shown in Figs. 4(a) and (b), where the gain and aperture efficiency for a fixed lens diameter (20, 40, and 60 λ) are obtained as a function of the number of spherical shells. In this figure, one can observe that

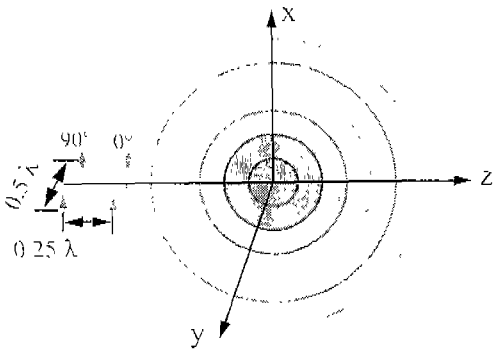

(a)

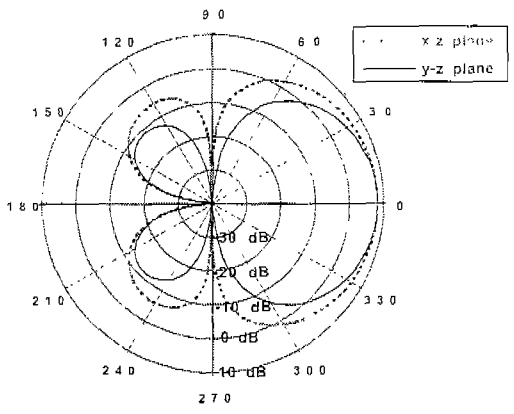

(b)

Fig. 3. (a) An end-fire array as a feed source for the Luneburg lens antenna. The end-fire array is located in the y-z plane, and the infinitesimal dipoles are oriented in the x-direction. (b) Gain patterns of the feed source in the x-z and y-z plane.

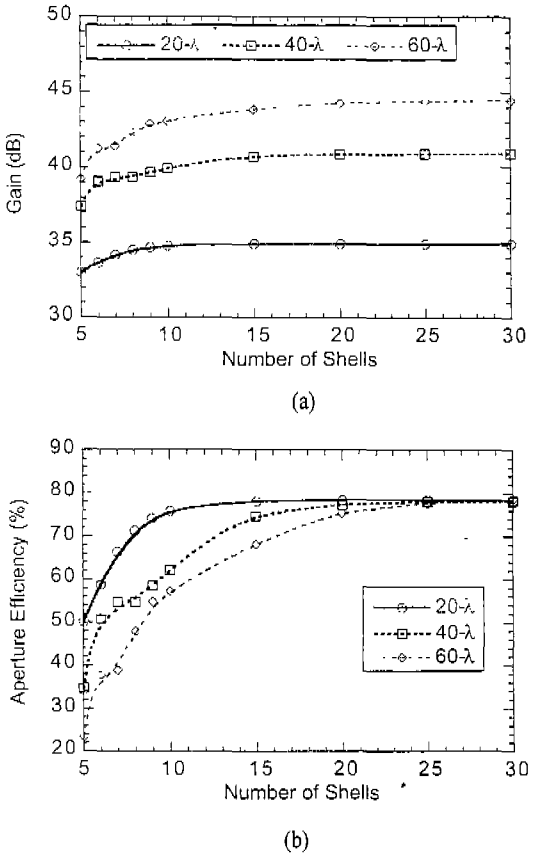

Fig. 4. (a) Gain and (b) aperture efficiency of the Luneburg lens antenna (20, 40, 60 λ diameter) as a function of the number of the spherical shells.

the gain and aperture efficiency become saturated with a finite number of spherical shells: e.g., ~10 shells for a 20-λ diameter lens, ~25 shells for a 60-λ diameter lens. This implies that a Luneburg lens antenna with a good performance can be implemented using multiple spherical shells of about 1 wavelength thickness, which contradicts the previous predictions that the shell thickness should be less than a quarter wavelength[10], but agrees with the results in [1]. In this calculation, the effects of air-gaps and the dielectric loss are not included. The maximum aperture efficiency for the selected feed source configuration is ~79 % (this includes the 7 % spill-over efficiency of the feed). The maximum aperture efficiency could be higher if the backward spill-over power is subtracted from the total radiated power.

The radiation patterns (in the x-z plane) of 60-λ Luneburg lenses with different number of shells are shown in Figs. 5(a) and (b). With a large number of shells, the radiation patterns of the Luneburg lens resembles those of the uniform circular aperture $(J_1(\rho)/\rho)$ where $\rho = ka\ \sin(\theta)$. With a smaller number of shells, the radiation pattern deviates from the $J_1(\rho)/\rho$ pattern at smaller θ angles. In Fig. 5(b), the side-lobe of the 5-shell lens increases first at ~4°. With 10-shells, the side lobe increases at ~12°, and with the 20-shell lens, the side-lobe level increased at ~32° due to finite number of shells.

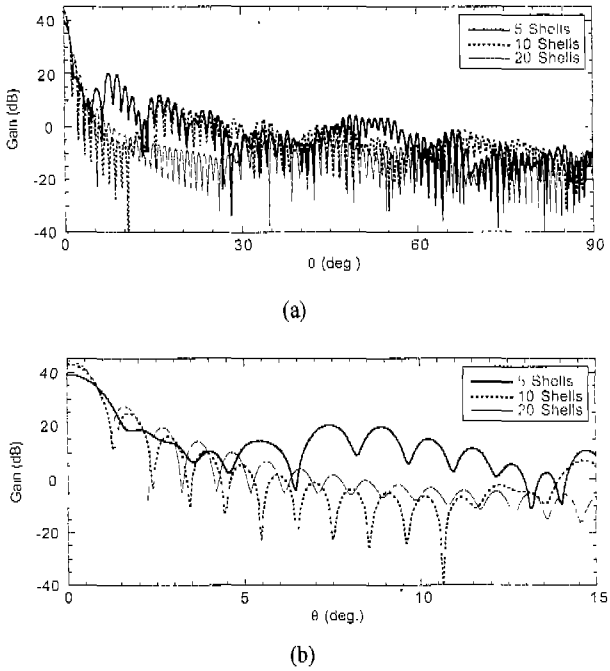

Fig. 5. (a) Gain patterns of the 60-λ Luneburg lens antenna in the x-z plane with different number of spherical shells (5, 10, 20 shells); (b) expanded plot of (a).

3-2 Effects of Air-gaps in the Luneburg Lens Antenna

Air-gaps between spherical shells may be unavoidable in the process of constructing the Luneburg lens with a finite number of spherical shells. The air-gaps critically affect the performance of the Luneburg lens antenna. When air-gaps are present, the performance of the lens deteriorates since the phase correction of the lens antenna becomes worse.

The gain and aperture efficiency variations of the Luneburg lenses with air-gaps are compared for a 60-λ diameter lens in Fig. 6. In these figures, the air-gaps, which are assumed to exist between every adjoining shells with an equal gap width, are presented in fractions of the wavelength. In Fig. 6, without the air-gaps, the gain improves by about 1.2 dB by increasing the number of shells from 10 to 20. As the air-gap increases, the gain for the 20-shell lens antenna drops much faster than that of the 10-shell lens; the gain becomes less than that of the 10-shell lens when air-gap is greater than 0.03 λ. Therefore, in practical design of the Luneburg lens antenna, trade-offs between the gain increase with more number of shells and the

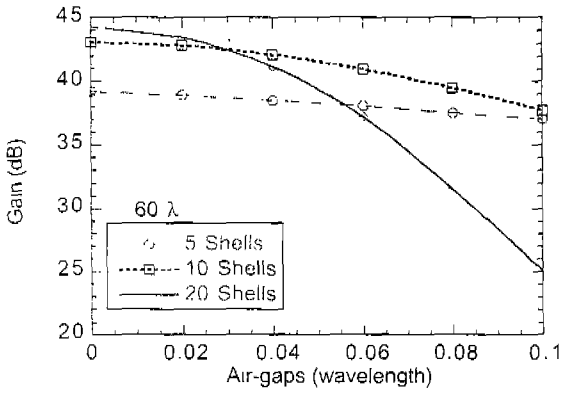

(a)

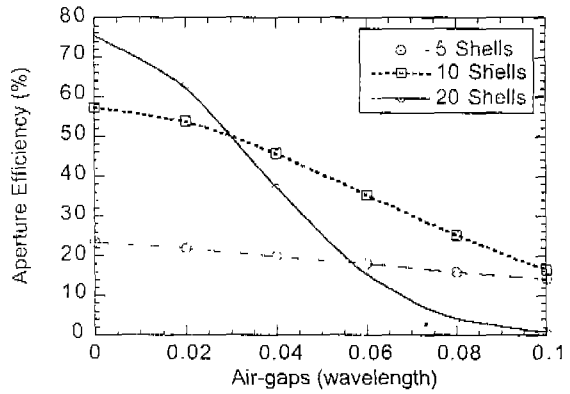

(b)

Fig. 6. Effects of air-gaps: (a) Gain and (b) aperture efficiency of the 60-λ diameter Luneburg lens for different number of shells(5, 10, 20 shells).

gain degradation due to air-gaps should be considered. At high frequencies, such as 60 GHz, these air-gap requirements may be rather stringent since 0.03 λ air-gap at this frequency is only 150 μm wide.

The radiation pattern variation without and with air-gaps for the 60-λ 20-shell Luneburg lens is shown in Figs. 7(a) and (b). The side-lobe level in the x-z plane is -17 dB down from the main lobe with no air-gap. The side-lobe level in the y-z plane is lower; i.e., -23 dB because of the feed pattern taper as shown in Fig. 3(b). As the air-gap increases the peak gain decreases. With the increased air-gaps, the pattern nulls are

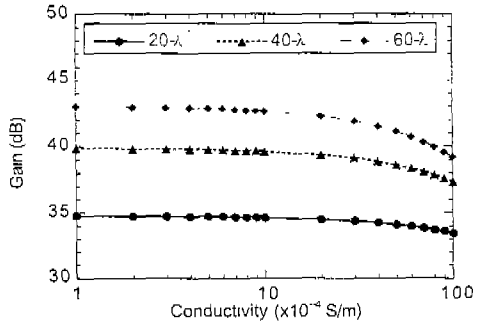

(a)

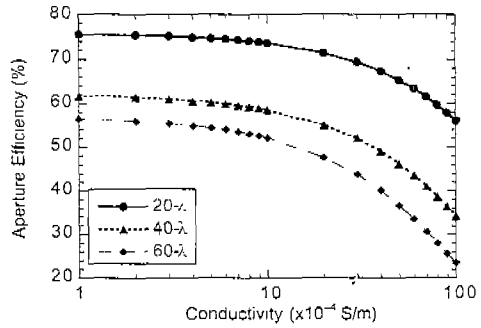

(b)

Fig. 8. (a) Gain and (b) aperture efficiency of the Luneburg lens (20, 40, 60-λ diameter) as a function of the dielectric loss.

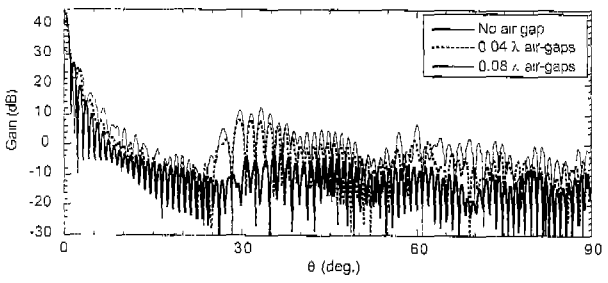

(a)

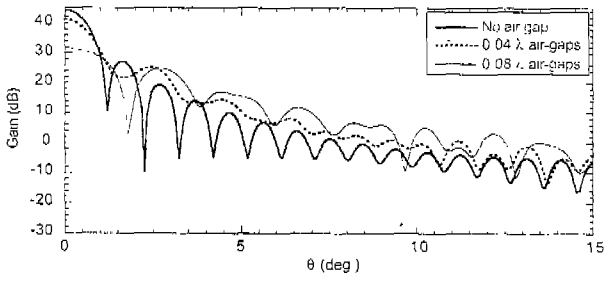

(b)

Fig. 7. (a) Gain patterns of the 60-λ diameter, 20-shell Luneburg lens antenna in the x-z plane as a function of the air-gap width; (b) expanded plot of (a).

smeared out as shown in Fig. 7(b), whereas the radiation pattern of the Luneburg lens antenna with no air-gap closely follows the $J_1(\rho)/\rho$ pattern of the uniform circular aperture.

3-3 Effects of Dielectric Loss

A Luneburg lens is usually fabricated using the dielectric material such as polystyrene or polyethylene. These dielectric materials have dielectric losses which are related to the imaginary part of the permittivity. The loss tangent of the polystyrene (tan $\delta = \varepsilon''/\varepsilon'$) is ~0.00033 at 10 GHz. The imaginary part of permittivity, ε'', can be related to the conductivity by $\sigma = \omega \varepsilon_0 \varepsilon''$; i.e., $\sigma \cong 2\times10^{-4}$ S/m at 10 GHz. At higher frequencies, the dielectric loss will be greater. The gain loss associated with the variation of the conductivity is plotted in Fig. 8. The Luneburg lens antenna is assumed to have 10 spherical shells. For example, with a 20-λ diameter lens, the gain difference between no loss and $\sigma = 1\times10^{-3}$ S/m is only ~0.13 dB. Therefore, it can be concluded that the significance of dielectric loss effects is less than that of the air-gap effects if low-loss dielectric material is used for lens fabrication. However, the gain loss can not be ignored at higher operating frequencies or using lossy dielectric materials.

Ⅳ. CONCLUSION

This paper has presented detailed engineering characterizations of Luneburg lens antennas. An advanced numerical technique has been utilized to perform comprehensive analysis. The technique can be used to study very large diameter (in excess of 80 wavelengths) Luneburg lens and many spherical layers (in excess of 40 layers), and it may handle most of the practical design interests of the Luneburg lens antenna. The numerical solution has been obtained using the eigenfunction expansion method with an adaptive convergence test.

A summary of important observations for the design of the Luneburg lens antennas are presented as follows: the gain and aperture efficiency improves by increasing the number of spherical shells, but they become saturated with ~1 λ thickness for each shell. The radiation pattern of Luneburg lens antenna resembles that of the uniform circular aperture ($J_1(\rho)/\rho$) with more spherical shells; with smaller number of shells, the radiation pattern deviates from $J_1(\rho)/\rho$ pattern at smaller θ angle. The air-gaps generally deteriorate the performance of the Luneburg lens; with more spherical shells, the air-volume is increased and lens gain drop is greater with a given gap width. The far-field pattern nulls may be smeared out with air-gaps. Therefore, there is a trade-off between general gain increase with more number of shells and performance degradation relating to air-gaps. The dielectric loss may not be as critical in performance as the air-gap effects if a low-loss lens material is used, but may become important at higher operating frequencies.

REFERENCES

[1] H. Shrank and J. R. Sanford, "A Luneberg Lens Update", *IEEE Antennas Propagat. Magazine*, vol. 37, no. 1, February, 1995.

[2] C. S. Silitonga, Y. Sugano, H. Sakura, M. Ohki, and S. Kozaki, "Optimum Variation of the Luneberg Lens for Electromagnetic Scattering Calculations", *Int. J. Electronics*, vol. 84, no. 6, pp. 625-633, 1998.

[3] J. R. Sanford, "Scattering by Spherically Stratified Microwave Lens Antennas", *IEEE Trans. Antennas Propagat.*, vol. 42, no. 5, pp. 690-698, May, 1994.

[4] M. A. Mitchell and J. R. Sanford, "Luneberg Lens Revival", *Electronics and Wireless World*, 95, pp. 456-458, May, 1989.

[5] R. K. *Luneburg, Mathematical Theory of Optics*, pp. 189-213, Brown University, Providence, Rhode Island, 1944; or pp. 182-187, University of California Press, Berkeley, 1964.

[6] C. T. Tai, "The Electromagnetic Theory of the Spherical Luneberg Lens", *Applied Scientific Research B*, vol. 7, no. 2, pp. 113-130, 1958.

[7] R. S. Elliott, *Antenna Theory and Design*, Prentice-Hall, Chapter 10, 1981.

[8] S. M. Morgan, "Generalization of Spherically Symmetric Lenses", *IRE Transactions on Antennas and Propagation*, AP-7(4), pp. 342-5, October, 1959.

[9] J. S. Hollis and M. W. Long, "A Luneburg Lens Scanning System", *IRE Transactions on Antennas and Propagation*, AP-5(1), pp. 21-25, January, 1957.

[10] E. F. Buckley, "Stepped-Index Luneburg Lenses", *Electronic Design*, pp. 86-89, April, 1960.

[11] L. C. Gunderson and G. T. Holmes, "Microwave Luneburg Lens", *Applied Optics*, vol. 7, no. 5, pp. 801-804, May, 1968.

[12] C. T. Tai, *Dyadic Green Functions in Electromagnetic Theory*, 2nd Edition, *IEEE PRESS Series on Electromagnetic Waves*, IEEE PRESS, New York, 1994.

[13] K. W. Kim and Y. Rahmat-Samii, "Antennas and Humans in Personal Communications: An Engineering Approach to the Interaction Evaluation", *Proceedings of the IEEE Engineering in Medicine and Biology Society*, Chicago, pp. 2488-2491, October, 1997.

[14] B. R. Johnson, "Light Scattering by a Multi-layered Sphere", *Applied Optics*, vol. 35, no. 18, pp. 3286-3296, June, 1996.

Kang Wook Kim

received B.S. and M.S. degrees in electrical engineering from Seoul National University in 1985 and 1987, respectively. In 1996, he received Ph.D. degree from the University of California, Los Angeles.

From 1987 to 1990, he worked as a researcher at the Korea Electrotechnology Research Institute, Changwon. From 1996 to 1998, he held a position as a post-doctoral researcher at the University of California, Los Angeles. From 1998 to 1999, he was employed as a microwave design engineer at P-Com, Inc., Campbell, California, designing commercial transceivers for digital microwave radios. Since 1999, he has been working as an RF design engineer at Narda DBS Microwave, an L-3 Communications Company, USA. He is currently engaged in research and development of microwave/mm-wave components and sub-systems for wireless and fiber optic communications. His research interests include antennas for wireless personal communications, EM interactions between human body and antennas, and plasma diagnostics using microwave/mm-wave components.